Increasing atmospheric humidity and CO_2 concentration alleviate forest mortality risk

Yanlan Liu[a], Anthony J. Parolari[b], Mukesh Kumar[a,1], Cheng-Wei Huang[c], Gabriel G. Katul[a,d], and Amilcare Porporato[d]

[a]Nicholas School of the Environment, Duke University, Durham, NC 27708; [b]Department of Civil, Construction, and Environmental Engineering, Marquette University, Milwaukee, WI 53233; [c]Department of Biology, University of New Mexico, Albuquerque, NM 87131; and [d]Department of Civil and Environmental Engineering, Duke University, Durham, NC 27708

Edited by Ignacio Rodriguez-Iturbe, Texas A&M University, College Station, TX, and approved July 21, 2017 (received for review March 23, 2017)

Climate-induced forest mortality is being increasingly observed throughout the globe. Alarmingly, it is expected to exacerbate under climate change due to shifting precipitation patterns and rising air temperature. However, the impact of concomitant changes in atmospheric humidity and CO_2 concentration through their influence on stomatal kinetics remains a subject of debate and inquiry. By using a dynamic soil–plant–atmosphere model, mortality risks associated with hydraulic failure and stomatal closure for 13 temperate and tropical forest biomes across the globe are analyzed. The mortality risk is evaluated in response to both individual and combined changes in precipitation amounts and their seasonal distribution, mean air temperature, specific humidity, and atmospheric CO_2 concentration. Model results show that the risk is predicted to significantly increase due to changes in precipitation and air temperature regime for the period 2050–2069. However, this increase may largely get alleviated by concurrent increases in atmospheric specific humidity and CO_2 concentration. The increase in mortality risk is expected to be higher for needleleaf forests than for broadleaf forests, as a result of disparity in hydraulic traits. These findings will facilitate decisions about intervention and management of different forest types under changing climate.

forest mortality | drought | climate change | hydraulic failure | stomatal closure

Forest mortality can lead to irreversible change in vegetation cover, thereby affecting many processes pertinent to water, carbon, and nutrient budgets (1). Multiple studies (2–10) have noted close association between forest mortality and water and heat stress, owing to shifting precipitation patterns and rising air temperature. However, the influence of concurrent changes in specific humidity (SH) and CO_2 concentration, which affect plant response to stress by altering stomatal kinetics (11), have not received similar attention. Although elevated CO_2 concentration is expected to promote future forest productivity (12), the extent to which it affects forest mortality in the context of water and heat stress remains a subject of inquiry. Short-term records (3, 4) and long-term manipulative field studies in forests such as the Free Air CO_2 Enrichment experiments (13–15) have tried to fill the knowledge gap; however, they do not cover the entire manifold of projected climate conditions. The goals of this study are to evaluate the individual and combined influence of projected changes in precipitation, temperature, SH, and CO_2 concentration on forest mortality risk and to investigate whether the response of mortality risk differs among plant functional types (PFTs).

Tree mortality may occur through several mechanisms, including hydraulic failure, carbon starvation, phloem transport limitation, and biotic attack (16, 17). Hydraulic failure is characterized as the malfunction of xylem water transport associated with cavitation, which is induced by low xylem water potential under limited soil water availability. Carbon starvation occurs when carbohydrate supply and storage cannot meet demand (17), which could result from low photosynthesis due to stomatal closure in response to low plant water potential and high atmospheric vapor pressure deficit (VPD). Reduced photosynthesis and plant water potential also pose limitations for phloem to maintain turgor pressure and may further impair phloem transport (18). Intense and prolonged stresses could weaken the defenses of forests to biotic attack (5) and may alter plant adaptation, seed production, and germination (2). Despite these mechanisms being far from thoroughly understood (17, 18), they primarily result from low plant water potential and restricted photosynthesis.

To quantify the risk of mortality induced by low plant water potential, previous studies (19, 20) used the safety margin [i.e., the difference between the minimum observed xylem water potential and the xylem water potential at 50% loss of conductivity (ψ_{50})]. Plants with narrower or more negative safety margins are considered to be more susceptible to hydraulic failure. The safety margin provides a static assessment of plant susceptibility to hydraulic failure, although its representativeness may be undermined by limited field observations. It has also been suggested that, instead of the minimum water potential plants reach, the duration plants operate under high percentage loss of conductivity could more likely distinguish mortality (21, 22). Here, a duration-based hydraulic failure risk (HFR) is introduced, which quantifies the fraction of days when the daily minimum xylem water potential ($\psi_{x,\min}$) falls below ψ_{50}. Because stomatal closure restricts photosynthesis (6, 17, 23), a stomatal closure risk (SCR) can also be formulated as the fraction of days on which stomata

Significance

The significance of forest mortality on ecosystem services, and water, carbon, and nutrient cycling is indubitable. While there is a general agreement that climate change-induced heat and drought stress is expected to intensify forest mortality, the concurrent influence of changes in atmospheric humidity and CO_2 concentration remains unclear. Here, the response of mortality risk to projected climate change is evaluated in 13 biomes across the globe. Our results show that increasing specific humidity and CO_2 concentration partially offset the intensification of risk by changing precipitation and air temperature. The risk response is also mediated by plant hydraulic traits. The study provides a mechanistic foundation for estimating future responses of forest mortality risk, which can facilitate ecosystem management.

Author contributions: Y.L., A.J.P., M.K., and A.P. designed research; Y.L. performed research; C.-W.H. and G.G.K. further developed model assumptions and scenarios; Y.L. analyzed data; and Y.L., A.J.P., M.K., C.-W.H., G.G.K., and A.P. wrote the paper.

Conflict of interest statement: Ignacio Rodriguez-Iturbe and A.P. were coauthors of a 2015 paper [Feng X, Porporato A, Rodriguez-Iturbe I (2015) Stochastic soil water balance under seasonal climates. Proc R Soc A 471: 20140623].

This article is a PNAS Direct Submission.

Freely available online through the PNAS open access option.

[1]To whom correspondence should be addressed. Email: mukesh.kumar@duke.edu.

This article contains supporting information online at www.pnas.org/lookup/suppl/doi:10.1073/pnas.1704811114/-/DCSupplemental.

are completely closed (*SI Appendix*, section S1). The aggregated mortality risk is then defined as the fraction of days with occurrence of either hydraulic failure or stomatal closure, two physiological states contributing to dieback and eventual mortality. Alternative quantifications of risk that account for stress duration and severity are also considered to test the robustness of the analysis here (*SI Appendix*, section S5).

The mortality risk is evaluated by using a soil–plant–atmosphere continuum (SPAC) model, which computes hourly dynamics of xylem water potential and stomatal conductance (Materials and Methods and *SI Appendix*, section S1). By comparing against observed mortality at four sites, the modeled risk is shown to capture the temporal variation of mortality in response to climate stressors (*SI Appendix*, section S3). The risks under historical and future climate scenarios are then evaluated for 13 temperate and tropical forest biomes across the globe (Fig. 1). The selected biomes cover a variety of climates and PFTs, including evergreen needleleaf forest (ENF), deciduous broadleaf forest (DBF), and evergreen broadleaf forest (EBF). The response of mortality risk to changes in the following climate characteristics is analyzed: mean annual precipitation (MAP), precipitation seasonality (PS), mean annual air temperature (T), mean annual atmospheric SH, and atmospheric CO_2 concentration. PS is quantified as the fraction of MAP that falls within the growing season. Changes in these climate conditions are obtained from the projection of Coupled Model Intercomparison Project Phase 5 (CMIP5) (Table S2) from 1986–2005 to 2050–2069.

Influence of Individual Changes in Climate Variables

Mortality risk is found to increase with reduced annual precipitation and a lower fraction of precipitation in the growing season. Reduced precipitation decreases plant water potential via low soil moisture, hence increasing HFR (Fig. 2*D*, horizontal axis). Meanwhile, low plant water potential also restricts stomatal conductance, hence increasing SCR (Fig. 2*A*, horizontal axis). Plants experience higher risk in the growing season than in the nongrowing season, due to low plant water potential and atmospheric aridity imposed by a high VPD. Given the same annual precipitation, more growing season precipitation (higher PS) generally decreases the risk (Fig. 2 *A* and *D*, vertical axis). Reduced precipitation during the nongrowing season typically does not increase the risk, as the stressed conditions mostly occur in the growing season.

Sensitivity of mortality risk to precipitation amount and seasonality varies across soil, plant, and climate conditions, as expected. For ENF in the western United States (Fig. 2*A* and biome 1 in Fig. 1), the risk is primarily controlled by annual precipitation amount when <400 mm. For wetter climates (MAP > 800 mm) with low growing season precipitation (PS < 0.2), seasonality becomes the dominant factor. Under the historical climate in this region, both precipitation amount and seasonality play significant roles in mortality risk. Although large uncertainties exist in the projected annual precipitation, CMIP5 models mostly predict lower PS in this region, which is likely to increase mortality risk. For DBF in the southeastern United States (Fig. 2*D* and biome 3 in Fig. 1), both precipitation amount and seasonality affect the risk over a wide range of climatic conditions. Although the risk generally decreases with higher PS when PS < 0.7, the trend reverses for PS > 0.8. As CMIP5 projections point to an increase in precipitation with little change in seasonality, mortality risk of this biome is expected to decrease under future precipitation patterns.

Modeled mortality risk increases with warming air temperature, but decreases with rising SH (Fig. 2 *B* and *E*) and CO_2 concentration (Fig. 2 *C* and *F*). Elevated temperature promotes water loss through higher VPD. Although stomata close in response to high VPD to prevent excessive water loss, the same action increases the risk of full stomatal closure. Increasing SH, on the other hand, offsets the increase of VPD by air temperature, hence attenuating intensified risks caused by warming. Under higher atmospheric CO_2 concentration, plants can operate at lower stomatal conductance to meet their biochemical demand for CO_2. This so-called "carbon fertilization effect" allows plants to enhance water-use efficiency, hence reducing the risks of both hydraulic failure and stomatal closure simultaneously. All three climate variables exhibit significant influence on mortality risk of ENF in the western United States and DBF in the southeastern United States. For the projected changes in temperature and SH (Fig. 2 *B* and *E*), the intensifying influence of rising air temperature overwhelms the opposing influence of rising SH, leading to higher VPD, and thus

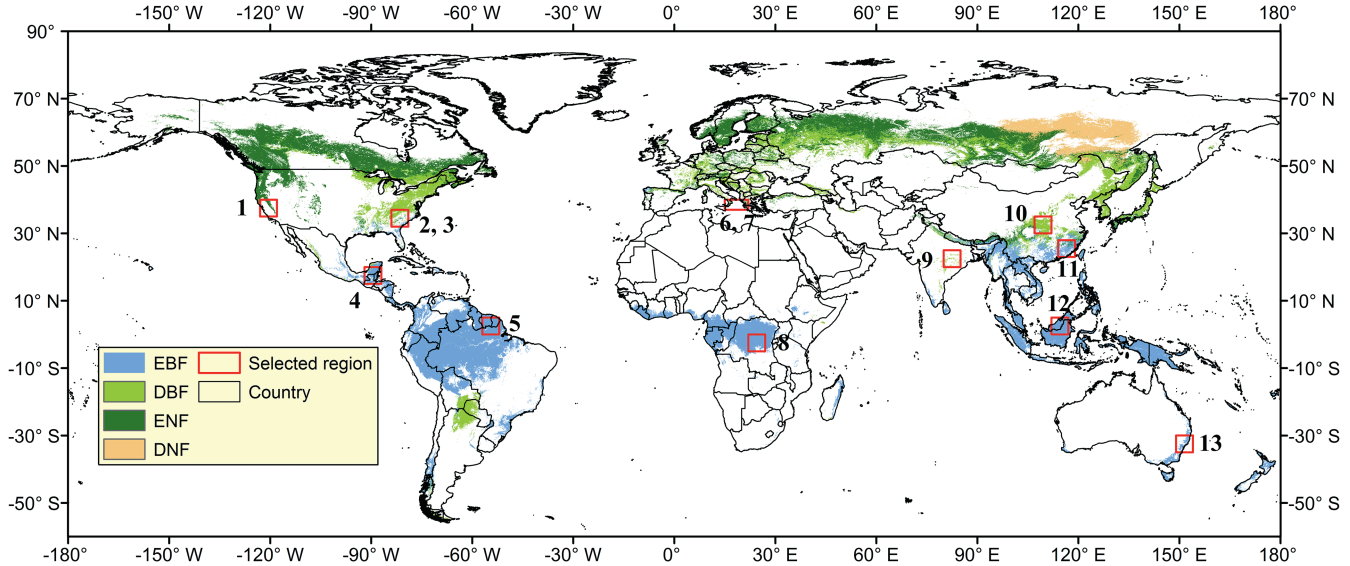

Fig. 1. Distribution of PFT and locations of the 13 investigated biomes. Biomes are the areas within the selected rectangular regions that are covered by a given PFT. PFTs shown in the map include evergreen broadleaf forest (EBF), deciduous broadleaf forest (DBF), evergreen needleleaf forest (ENF), and deciduous needleleaf forest (DNF).

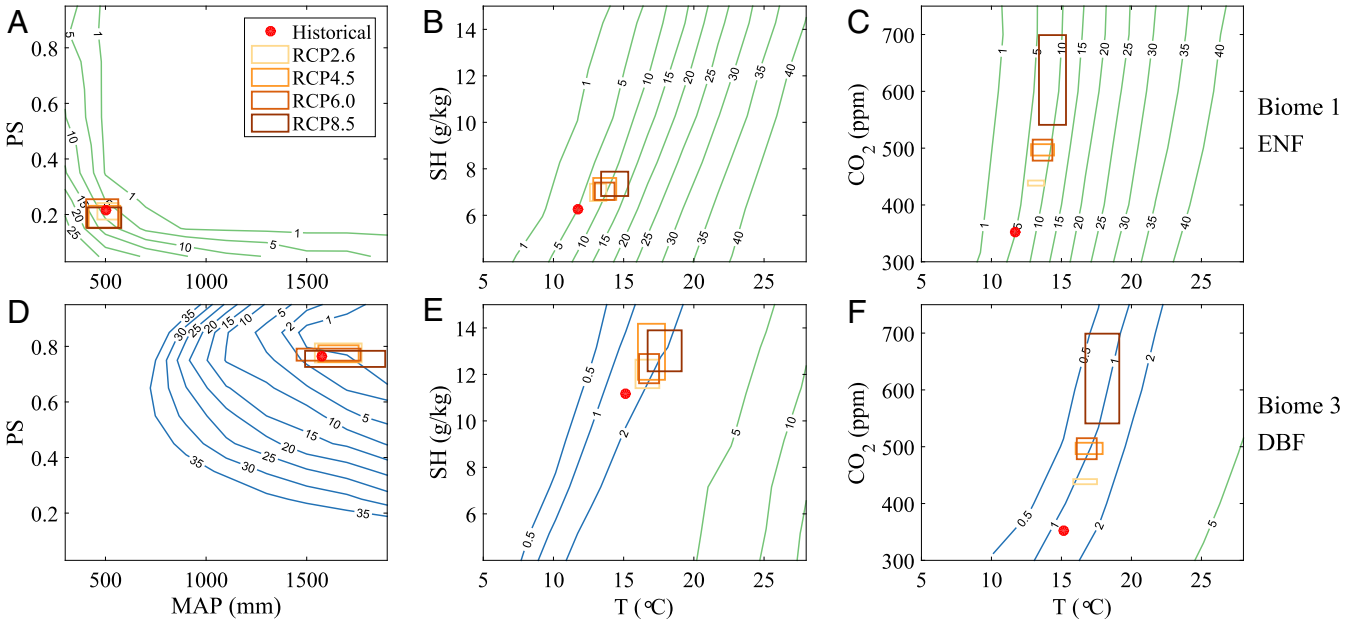

Fig. 2. Responses of mortality risk to individual changes in MAP, PS, T, SH, and CO_2 concentration for ENF in the western United States (*A*–*C*) and DBF in the southeastern United States (*D*–*F*). PS is quantified as the fraction of MAP that falls within the growing season. Changes in MAP and PS are incorporated in daily precipitation time series through their impact on the statistical distribution of stochastic precipitation; changes in T, SH, and CO_2 are incorporated uniformly throughout the year, keeping the intraannual patterns unchanged. Numbers on the contours denote risk magnitude (%). Predicted ranges by multimodels under the four representative concentration pathway (RCP) scenarios are illustrated by rectangles. Blue and green contours represent risks due to hydraulic failure and stomatal closure, respectively.

higher risk. Remarkably, elevated CO_2 concentrations offset the intensified risk imposed by elevated temperature (Fig. 2 *C* and *F*).

Despite the similar patterns of response to climate change, sources of risk in the two biomes (Fig. 2) are markedly different. Under both historical and projected climates, the risk for the ENF in the western United States mostly originates from stomatal closure. The risk for the DBF in the southeastern United States mostly originates from hydraulic failure. However, under extremely high air temperature (annual mean $> 23°C$) in the DBF, high VPD induces full stomatal closure, resulting in a switch from HFR to SCR (Fig. 2 *E* and *F*). The different sources of risk for these two biomes can be attributed to their response strategies under stress, which are controlled by their hydraulic traits. ENF consists of conifers, which mostly operate with a wide safety margin ($\psi_{x,min} - \psi_{50}$) (19) and exhibit an isohydric strategy under stress (16) (i.e., restricting transpiration by reducing stomatal conductance while maintaining high water potential to prevent runaway cavitation; *SI Appendix*, Fig. S3). Owing to this conservative water use strategy and the wide safety margin, isohydric conifers are more susceptible to SCR than HFR. In contrast, DBF consists of angiosperms, which operate with a narrower safety margin (19) and largely use an anisohydric strategy under stress (16) (i.e., stomata remain open to sustain photosynthesis at the expense of decreased water potential; Fig. S3). With this less conservative water use strategy and a narrow safety margin, anisohydric DBFs are more susceptible to HFR than SCR. These contrasting stress responses have been widely reported (16, 19, 24). Previous studies have also suggested hydraulic failure as the major mechanism in an aspen (angiosperm) mortality event (8) and near-zero stomatal conductance as the main contributor to conifer mortality events (16, 23). It is to be noted that large variations in hydraulic traits exist within each PFT, and the results presented here are based on the average traits of species falling within a PFT and climate type in a given biome.

Influence of Combined Changes in Climate Variables

Based on the CMIP5 projections of four RCP scenarios in all 13 biomes (*SI Appendix*, Fig. S6), the response of mortality risk to changes in three combinations of climate conditions are examined (Fig. 3): (*i*) P+T; (*ii*) P+T+SH; and (*iii*) P+T+SH+CO_2. Here, changes in P include combined changes in MAP and PS. For the 13 investigated biomes, on average, shifting precipitation patterns and rising temperature projected by RCP4.5 are found to intensify the risk by 158.8% for the period 2050–2069 relative to the historical risk. This increase in risk is consistent with previous studies highlighting the exacerbating effects of higher temperature (1, 3–7). However, by incorporating increases in SH, the risk decreases by 46.6%. More remarkably, the risk drops an additional 91.2% under the added influence of elevated CO_2 concentration. In aggregate, changes in all four climate conditions increase the risk by 21.0% on average, which is much lower than the increase of 158.8% when only the changes in precipitation and air temperature are considered. Under high emission scenarios (RCP6.0 and RCP8.5), elevated humidity and CO_2 concentration might even overwhelm the effects of higher temperature, possibly resulting in a lower risk than the historical level (Fig. 3). These alleviating effects are robust across alternative risk measures (*SI Appendix*, Table S6 and Fig. S14). The alleviating effect of increasing atmospheric CO_2 concentration is in line with a reported decrease in stomatal conductance and increase in water use efficiency across various climate regions and species (2, 25–29).

On average, the combined changes of P+T+SH+CO_2 in RCP4.5 are found to increase the mortality risks by 101.1%, −18.3%, and 19.6% for ENF, DBF, and EBF biomes respectively (Fig. 4). The significantly higher increase for ENF compared with the other two PFTs results from their distinct risk sources (Fig. 4). SCR, the primary risk source for ENF, shows notably higher sensitivity to air temperature rise than HFR. Specifically, for a 1 °C increase in air temperature from historical climates, HFR and SCR are estimated to increase by 23.5% and 125.1%. Remarkably, the increase in SCR is close to the

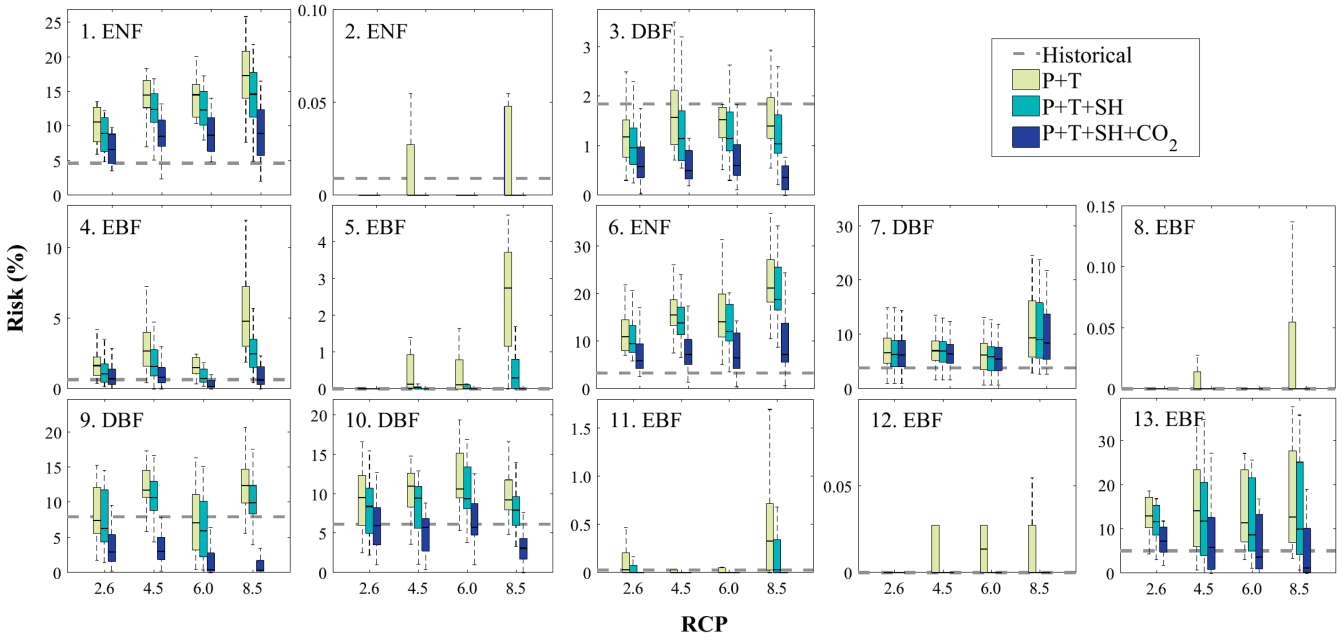

Fig. 3. Response of mortality risk to combined changes in climate variables. P+T includes changes in MAP, PS, and air temperature; P+T+SH includes additional changes in SH; and P+T+SH+CO_2 includes additional changes in atmospheric CO_2 concentration. Gray dashed lines in the subplots show the risks under historical climates. Upper and lower boundaries of the boxes correspond to the 25th and 75th quantiles of the risk based on multimodel projections in each RCP scenario. Numbers in the subplots correspond to the biome locations in Fig. 1.

previously reported 116.3% $°C^{-1}$ increase in die-off events of *Pinus edulis* (4), a conifer species likely threatened by SCR. From a mechanistic perspective, elevated temperature increases VPD and reduces stomatal conductance. This restricts carbon assimilation but promotes water loss, which results in a higher probability of full stomatal closure (i.e., higher SCR). The increase in HFR is smaller, as the reduction in stomatal conductance partly alleviates the increase in water loss due to increased VPD. Under projected changes of precipitation and VPD in RCP4.5, HFR increases by 135.5% on average, while SCR increases by 305.8%. When CO_2 is also considered, the aggregate changes are −8.6% and 83.7% for HFR and SCR, respectively. These findings imply a larger increase in mortality risk of ENFs, more specifically of isohydric species, than other PFTs under changes in the considered climate conditions.

Discussion and Implications

The study evaluates how projected climate change will affect mortality risks and how the risks may be mediated by different PFTs across the globe. In this regard, the study introduces a measure of mortality risk that accounts for the duration that plants operate under high percentage loss of conductivity or stomatal closure. Although large uncertainty exists in the exact physiological mechanisms that cause mortality (17, 18), the proposed mortality risk measure captures two of the fundamental causes (i.e., low water potential and severely restricted carbon assimilation) which contribute to the downstream mortality mechanisms. Notably, the quantification of mortality is made possible by synergistic coupling of multiple prior submodels connecting plant physiological status to hydrological and meteorological conditions. This coupling allows the SPAC model to resolve hourly dynamics of xylem water potential and stomatal conductance, the variables required to evaluate mortality risk (*SI Appendix*, sections S1 and S5). For example, by accounting for the feedback between evapotranspiration and atmospheric boundary layer (ABL) development, the SPAC model is able to simulate a physically consistent hourly dynamic of air temperature and SH during droughts. During drought, when evapotranspiration is restricted by low soil moisture, the model partitions a larger fraction of incoming energy into sensible heat, thus enhancing the ABL and raising the temperature during daytime. This evapotranspiration–ABL coupling allows SPAC to consider the cooccurrence of extreme drought and heat stress, which has been pointed out as the main environmental trigger of tree mortality (3–5, 7). The SPAC model also uses an optimization-based stomatal conductance representation that accounts for the effect of plant hydraulic limitation (*SI Appendix*, section S1). The representation is an advantage over several widely used dynamic global vegetation models, where

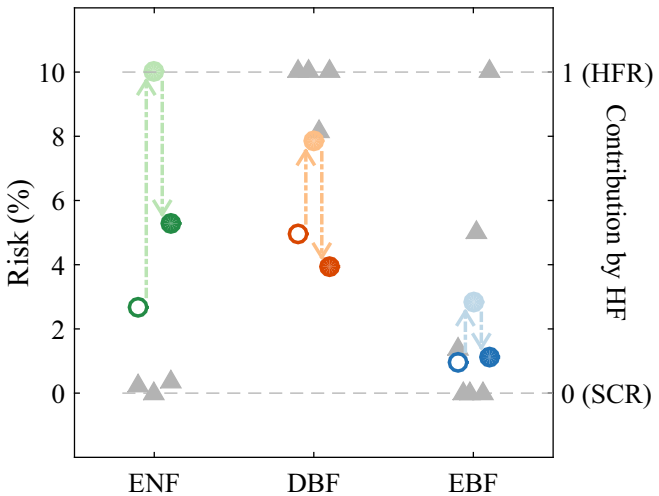

Fig. 4. Average risk under historical climates (open circles), changes in P+T (light filled circles), and changes in P+T+SH+CO_2 (dark filled circles) for each PFT based on RCP4.5. Gray filled triangles denote the relative contribution of hydraulic failure (HF) to the mortality risk (i.e., 1 denotes that all of the risk is due to HF, and 0 denotes all of the risk is from stomatal closure).

the stomatal regulation is disconnected or empirically connected with soil water stress (6, 21). Many of these semiempirical models are derived from observations under ambient CO_2 concentration, and their parameter values are subject to change in an elevated CO_2 environment (11), thus undermining their efficacy under future climate. In contrast, the optimization-based stomatal regulation model used here has been demonstrated to predict stomatal response to stress under both historical and elevated CO_2 concentration (30).

Although the modeled risk shows strong correspondence with observed mortality (*SI Appendix*, section S3), the estimated risk should be interpreted with care. Given the uncertainties inherent in model structure and parameters, and the complexity of the forest ecosystem, it is unrealistic to accurately assess the exact magnitude of mortality risk. Large variations in plant hydraulic traits, tree height, diameter at breast height, and stand density (31, 32) may impact the actual mortality risk. Sensitivity of mortality risk to aforementioned factors and to uncertainties in model structure are examined (*SI Appendix*, section S4). Results indicate that, despite their influence on the magnitude of mortality risk, the alleviating effect of increasing SH and CO_2 concentration is still found to be robust. Notably, actual mortality risk may also be altered by forest fire frequency and insect outbreak, rooting profile, seed production, community-level competition, local acclimation to drought, and adaption to long-term climate change (33–36), factors whose characterization is still fraught with uncertainties (37). Their impacts in relation to the direct influence of climate conditions discussed here deserve further investigation. However, independent of these indirect influences, results reported here demonstrate a ubiquitous and robust alleviating effect of elevated atmospheric humidity and CO_2 concentration, which is comparable in magnitude to the intensifying effect of changes in precipitation patterns and air temperature. The combined influence of changes in these climate variables on mortality risk is also strongly mediated by plant hydraulic traits. These results highlight that ignoring the influence of elevated atmospheric humidity and CO_2 concentration may lead to overestimation of future forest mortality risk.

Materials and Methods

SPAC Model. The SPAC model consists of three process components: a soil–water balance; a plant water transport that is based on cohesion–tension theory and associated hydraulic properties; and an ABL development model that permits evapotranspiration to alter the height, temperature, and SH of the boundary layer (*SI Appendix*, section S1 and Fig. S1). Soil is characterized as a two-layer bucket, where the soil moisture is controlled by precipitation, interception, vertical flux between the two soil layers, deep percolation, soil evaporation, and plant root extraction. Water transport within plants is modeled as a resistance system with no capacitance. Water vapor and CO_2 exchange at the leaf level are modeled by combining Fickian diffusion of gases and the Farquahar photosynthesis model (38, 39), where the stomatal kinetics are determined by optimizing carbon gain while minimizing water losses (11). The stomatal conductance is affected by both atmospheric conditions and plant water status. The water flux through the soil–plant–atmosphere system is solved given soil and atmospheric conditions. Subdaily temperature and SH are obtained from the ABL development model. The energy and mass components in ABL development are affected by feedback of total water flux from the ground surface (40), including interception, soil evaporation, and plant transpiration. The coupled SPAC model simulates ecohydrologic states at an hourly interval.

Soil and Vegetation Properties. Based on the global land cover type from the moderate imaging spectroradiometer (MODIS; MCD12C1) (41), 13 forest biomes were selected across the globe. The biomes cover three PFTs and a variety of climate types (Fig. 1 and *SI Appendix*, Table S1) with MAP ranging from 500 to 3,000 mm. Regions with shallow groundwater (42) and snow-dominated climate (43) were avoided, as the influence of groundwater and snow is not considered in the model. The SPAC model in each biome was parameterized with local soil and representative plant properties. Soil texture compositions were obtained from the Harmonized World Soils Database (44). Soil hydraulic properties were calculated based on the generalized statistical relations (45). The annual cycle of the Leaf Area Index (LAI) was extracted from the level-4 MODIS global LAI and Fraction of Photosynthetically Active Radiation product (MCD15A2) (46). Plant hydraulic traits were obtained from a global database containing hydraulic traits of 866 species (47). Photosynthetic parameters were derived from a cross-species study (48). Stomatal optimization parameters were obtained based on a metaanalysis study across PFTs and climates reported in a previous study (49). These plant properties were obtained at a biome level by averaging the properties of trees belonging to the same PFT and climate type (47) as found in the given biome.

Historical and Projected Climates. The SPAC model in each biome is forced by local daily climate, including stochastic precipitation, net shortwave radiation, and initial and boundary conditions of potential temperature and SH of ABL. At the beginning of each day, the ABL is reset with the corresponding initial and boundary conditions. The stochastic precipitation is represented as a marked Poisson process characterized by frequency and mean rainfall depth statistics (50). Daily historical climates are calculated based on the National Centers for Environmental Prediction (NCEP)/National Center for Atmospheric Research (NCAR) reanalysis data (51) from 1986 to 2005. Projected climate changes are obtained from multimodel outputs of CMIP5 experiments under four RCP scenarios (Table S2). For each model under each RCP scenario, changes in climate variables are quantified as the difference between the averages for 1986–2005 and 2050–2069. Future precipitation statistics and other climate forcings for the model are generated by incorporating these changes into the historical climates from NCEP/NCAR (*SI Appendix*, section S2) to eliminate the influence of biases in climate model outputs (52). Historical and future atmospheric CO_2 concentrations under the four RCP scenarios are provided in ref. 53.

Experimental Design and Statistics. The mortality risk under a given climate was quantified based on plant dynamics by running the SPAC model at hourly resolution for 30 annual ensembles after a 5-y warm-up period. Influence of changes in each individual climate variable was analyzed by keeping the others the same, while only changing the target climate variable. Influence of combined changes in climate variables as projected by multimodels were grouped together to evaluate the overall response of mortality risk under each RCP scenario. Each reported change in risk is the average of changes of all of the biomes, unless stated otherwise. Change in each biome was calculated as the difference between the historical risk and the future risk (i.e., the average risk based on multimodel projections), in proportion to the historical risk. Biomes with historical risks $<0.01\%$ were excluded from the statistics.

Note. Details on model formulation, data processing, model validation, sensitivity analyses, and alternative quantifications of risks are provided in *SI Appendix*.

ACKNOWLEDGMENTS. We thank the National Aeronautics and Space Administration Earth Observing System Data and Information System Land Processes Distributed Active Archive Center for maintaining and providing the MODIS data; the National Oceanic and Atmospheric Administration/Office of Oceanic and Atmospheric Research/Earth System Research Laboratory Physical Sciences Division for providing NCEP data; the World Climate Research Program's Working Group on Coupled Modeling, which is responsible for CMIP; the climate modeling groups (listed in *SI Appendix*, Table S2) for providing their model outputs; and the Numerical Terradynamic Simulation Group at University of Montana and Max Planck Institute for Biogeochemistry for sharing their data. M.K. was supported by National Science Foundation (NSF) Grant EAR-1454983. M.K. and A.P. were supported by NSF Grant EAR-1331846. A.P. and G.G.K. were supported by NSF Grant DGE-1068871. A.P. was additionally supported by NSF Grants EAR-1316258 and FESD EAR-1338694. G.G.K. was additionally supported by NSF Grant EAR-134470 and US Department of Energy Grant DE-SC0011461. C.-W.H. was supported by NSF Grant DEB-1557176.

1. Allen CD, et al. (2010) A global overview of drought and heat-induced tree mortality reveals emerging climate change risks for forests. *Forest Ecol Manag* 259:660–684.
2. Allen CD, Breshears DD, McDowell NG (2015) On underestimation of global vulnerability to tree mortality and forest die–off from hotter drought in the Anthropocene. *Ecosphere* 6:1–55.
3. Breshears DD, et al. (2005) Regional vegetation die–off in response to global–change–type drought. *Proc Natl Acad Sci USA* 102:15144–15148.
4. Adams HD, et al. (2009) Temperature sensitivity of drought-induced tree mortality portends increased regional die–off under global–change–type drought. *Proc Natl Acad Sci USA* 106:7063–7066.

5. Williams AP, et al. (2013) Temperature as a potent driver of regional forest drought stress and tree mortality. *Nat Clim Change* 3:292–297.
6. McDowell NG, et al. (2015) Multi–scale predictions of massive conifer mortality due to chronic temperature rise. *Nat Clim Change* 6:295–300.
7. Anderegg WRL, Kane JM, Anderegg LDL (2013) Consequences of widespread tree mortality triggered by drought and temperature stress. *Nat Clim Change* 3: 30–36.
8. Anderegg WRL, et al. (2012) The roles of hydraulic and carbon stress in a widespread climate-induced forest die–off. *Proc Natl Acad Sci USA* 109:233–237.
9. Anderegg LDL, Anderegg WRL, Abatzoglou J, Hausladen AM, Berry JA (2013) Drought characteristics' role in widespread aspen forest mortality across Colorado, USA. *Glob Change Biol* 19:1526–1537.
10. Parolari AJ, Katul GG, Porporato A (2014) An ecohydrological perspective on drought–induced forest mortality. *J Geophys Res Biogeosci* 119:965–981.
11. Katul G, Manzoni S, Palmroth S, Oren R (2009) A stomatal optimization theory to describe the effects of atmospheric CO_2 on leaf photosynthesis and transpiration. *Ann Bot* 105:431–442.
12. Schimel D, Stephens BB, Fisher JB (2015) Effect of increasing CO_2 on the terrestrial carbon cycle. *Proc Natl Acad Sci USA* 112:436–441.
13. Norby RJ, Zak DR (2011) Ecological lessons from free-air CO_2 enrichment (FACE) experiments. *Annu Rev Ecol Evol Systemat* 42:181–203.
14. Ainsworth EA, Long SP (2005) What have we learned from 15 years of free–air CO_2 enrichment (FACE)? A meta–analytic review of the responses of photosynthesis, canopy properties and plant production to rising CO_2. *New Phytol* 165: 351–372.
15. EIlsworth DS, et al. (2004) Photosynthesis, carboxylation and leaf nitrogen responses of 16 species to elevated pCO_2 across four free–air CO_2 enrichment experiments in forest, grassland and desert. *Glob Change Biol* 10:2121–2138.
16. McDowell N, et al. (2008) Mechanisms of plant survival and mortality during drought: Why do some plants survive while others succumb to drought? *New Phytol* 178: 719–739.
17. McDowell NG, et al. (2011) The interdependence of mechanisms underlying climate–driven vegetation mortality. *Trends Ecol Evol* 26:523–532.
18. Sala A, Piper F, Hoch G (2010) Physiological mechanisms of drought–induced tree mortality are far from being resolved. *New Phytol* 186:274–281.
19. Choat B, et al. (2012) Global convergence in the vulnerability of forests to drought. *Nature* 491:752–755.
20. Delzon S, Cochard H (2014) Recent advances in tree hydraulics highlight the ecological significance of the hydraulic safety margin. *New Phytol* 203:355–358.
21. McDowell NG, et al. (2013) Evaluating theories of drought–induced vegetation mortality using a multimodel–experiment framework. *New Phytol* 200:304–321.
22. Sperry JS, Love DM (2015) What plant hydraulics can tell us about responses to climate–change droughts. *New Phytol* 207:14–27.
23. Poyatos R, Aguadé D, Galiano L, Mencuccini M, Martínez-Vilalta J (2013) Drought–induced defoliation and long periods of near-zero gas exchange play a key role in accentuating metabolic decline of Scots pine. *New Phytol* 200:388–401.
24. McDowell NG (2011) Mechanisms linking drought, hydraulics, carbon metabolism, and vegetation mortality. *Plant Physiol* 155:1051–1059.
25. Ainsworth EA, Rogers A (2007) The response of photosynthesis and stomatal conductance to rising CO_2: Mechanisms and environmental interactions. *Plant Cell Environ* 30:258–270.
26. Brodribb TJ, McAdam SAM, Jordan GJ, Feild TS (2009) Evolution of stomatal responsiveness to CO_2 and optimization of water–use efficiency among land plants. *New Phytol* 183:839–847.
27. Lammertsma EI, et al. (2011) Global CO_2 rise leads to reduced maximum stomatal conductance in Florida vegetation. *Proc Natl Acad Sci USA* 108:4035–4040.
28. Keenan TF, et al. (2013) Increase in forest water–use efficiency as atmospheric carbon dioxide concentrations rise. *Nature* 499:324–327.
29. Drake BL, Hanson DT, Lowrey TK, Sharp ZD (2017) The carbon fertilization effect over a century of anthropogenic CO_2 emissions: Higher intracellular CO_2 and more drought resistance among invasive and native grass species contrasts with increased water use efficiency for woody plants in the US Southwest. *Glob Change Biol* 23: 782–792.
30. Katul GG, Palmroth S, Oren R (2009) Leaf stomatal responses to vapour pressure deficit under current and CO_2–enriched atmosphere explained by the economics of gas exchange. *Plant Cel Environ* 32:968–979.
31. Rowland L, et al. (2015) Death from drought in tropical forests is triggered by hydraulics not carbon starvation. *Nature* 528:119–122.
32. Bottero A, et al. (2017) Density–dependent vulnerability of forest ecosystems to drought. *J Appl Ecol*, 10.1111/1365-2664.12847.
33. Clark JS, et al. (2016) The impacts of increasing drought on forest dynamics, structure, and biodiversity in the United States. *Glob Change Biol* 22:2329–2352.
34. Wolf A, Anderegg WR, Pacala SW (2016) Optimal stomatal behavior with competition for water and risk of hydraulic impairment. *Proc Natl Acad Sci USA* 113:E7222–E7230.
35. Wolfe BT, Sperry JS, Kursar TA (2016) Does leaf shedding protect stems from cavitation during seasonal droughts? A test of the hydraulic fuse hypothesis. *New Phytol* 212:1007–1018.
36. Jump AS, et al. (2017) Structural overshoot of tree growth with climate variability and the global spectrum of drought–induced forest dieback. *Glob Change Biol*, 10.1111/gcb.13636.
37. Norby RJ, et al. (2005) Forest response to elevated CO2 is conserved across a broad range of productivity. *Proc Natl Acad Sci USA* 102:18052–18056.
38. Collatz GJ, Ball JT, Grivet C, Berry JA (1991) Physiological and environmental regulation of stomatal conductance, photosynthesis and transpiration: A model that includes a laminar boundary layer. *Agric For Meteorol* 54:107–136.
39. Farquhar GD, Caemmerer Sv, Berry JA (1980) A biochemical model of photosynthetic CO_2 assimilation in leaves of C3 species. *Planta* 149:78–90.
40. de Arellano JVG, van Heerwaarden CC, Lelieveld J (2012) Modelled suppression of boundary–layer clouds by plants in a CO_2–rich atmosphere. *Nat Geosci* 5:701–704.
41. National Aeronautics and Space Administration Land Process Distributed Active Archive Center (2013) Land Cover Type Yearly L3 Global 0.05Deg Climate Modeling Grid. (NASA Earth Observing System Data and Information System Land Processes Distributed Active Archive Center, US Geological Survey Earth Resources Observation and Science Center, Sioux Falls, SD), Version 051. Available at https://lpdaac.usgs.gov/dataset_discovery/modis/modis_products_table/mcd12c1. Accessed June 21, 2016.
42. Fan Y, Li H, Miguez-Macho G (2013) Global patterns of groundwater table depth. *Science* 339:940–943.
43. Kottek M, Grieser J, Beck C, Rudolf B, Rubel F (2006) World map of the Köppen-Geiger climate classification updated. *Meteorol Z* 15:259–263.
44. Food and Agriculture Organization of the United Nations (2009) Harmonized World Soil Database (Food and Agriculture Organization of the United Nations, Rome), Version 1.2. Available at www.fao.org/soils-portal/soil-survey/soil-maps-and-databases/harmonized-world-soil-database-v12/en/. Accessed June 22, 2016.
45. Saxton KE, Rawls WJ, Romberger JS, Papendick RI (1986) Estimating generalized soil–water characteristics from texture. *Soil Sci Soc Am J* 50:1031–1036.
46. National Aeronautics and Space Administration Land Process Distributed Active Archive Center (2016) Leaf Area Index—Fraction of Photosynthetically Active Radiation 8-Day L4 Global 1km. NASA Earth Observing System Data and Information System Land Processes Distributed Active Archive Center (US Geological Survey Earth Resources Observation and Science Center, Sioux Falls, SD), Version 005. Available at https://lpdaac.usgs.gov/dataset_discovery/modis/modis_products_table/mcd15a2. Accessed June 23, 2016.
47. Kattge J, et al. (2011) TRY—a global database of plant traits. *Glob Change Biol* 17:2905–2935.
48. Medlyn BE, et al. (2002) Temperature response of parameters of a biochemically based model of photosynthesis. II. A review of experimental data. *Plant Cell Environ* 25:1167–1179.
49. Manzoni S, et al. (2011) Optimizing stomatal conductance for maximum carbon gain under water stress: A meta–analysis across plant functional types and climates. *Funct Ecol* 25:456–467.
50. Rodríguez-Iturbe I, Porporato A (2007) *Ecohydrology of Water–Controlled Ecosystems: Soil Moisture and Plant Dynamics* (Cambridge Univ Press, Cambridge, UK).
51. Kalnay E, et al. (1996) The NCEP/NCAR 40-year reanalysis project. *Bull Am Meteorol Soc* 77:437–471.
52. Knutti R, Furrer R, Tebaldi C, Cermak J, Meehl GA (2010) Challenges in combining projections from multiple climate models. *J Clim* 23:2739–2758.
53. Meinshausen M, et al. (2011) The RCP greenhouse gas concentrations and their extensions from 1765 to 2300. *Climatic change* 109:213–241.